Quasar lenses in the south: searches over the DES public footprint

Adriano Agnello [1,2]★ and Chiara Spiniello [1,3]

[1]*European Southern Observatory, Karl-Schwarzschild-Strasse 2, D-85748 Garching, Germany*
[2]*DARK, Niels-Bohr Institute, Lyngbyvej 2, DK-2100 Copenhagen, Denmark*
[3]*INAF – Osservatorio Astronomico di Capodimonte, Salita Moiariello, 16, I-80131 Napoli, Italy*

ABSTRACT

We have scanned 5000 deg^2 of Southern Sky to search for strongly lensed quasars with five methods, all source oriented, but based on different assumptions and selection criteria. We present a list of high-grade candidates from each method (totalling 98 unique, new candidates), to facilitate follow-up spectroscopic campaigns, including two previously unknown quadruplets, WG 210014.9-445206.4 and WG 021416.37-210535.3. We analyse morphological searches based on *Gaia* multiplet detection and astrometric offsets, fibre-spectroscopic preselection, and X-ray and radio pre-selection. The performance and complementarity of the methods are evaluated on a common sample of known lenses in the Dark Energy Survey public Data Release 1 (DR1) footprint. We recovered in total 13 known lenses, of which 8 are quadruplets. Morphological and colour selection of objects, from the *WISE* and *Gaia*-DR2 surveys, recovers most of those known lenses, but searches in the radio and X-ray cover regimes that are beyond the completeness of *Gaia*. Given the footprint, pre-selection, and depth limits, the current number of quads indicates that the union of these searches is complete, and the expected purity on high-grade candidates is ≈60 per cent. Ongoing, spectroscopic campaigns confirm this estimate.

Key words: catalogues – galaxies: formation – dark matter.

1 INTRODUCTION

Sizeable samples of gravitationally lensed quasars, spanning a range in redshift, image separation, and mass, are essential to various scientific purposes. However, these objects are extremely rare: according to Oguri & Marshall (2010, hereafter OM10), one in ≈10^4 quasars is strongly lensed. One of the first efforts to build a large and well-studied statistical sample of strong gravitationallensed quasars has been made by The Cosmic Lens All-Sky Survey (CLASS; Myers et al. 2003). CLASS has obtained high-resolution radio images from the Very Large Array (VLA; at 8.4 GHz) of over 13 000 flat-spectrum radio sources, finding 22 radio-loud lenses. However, in radio lens surveys like CLASS, the redshift distribution of the flat-spectrum sources is poorly constrained (e.g. Muñoz et al. 2003). Only with the advent of the Sloan Digital Sky Survey (SDSS; York et al. 2000), which in its 14th Data Release confirmed 526 356 quasars spectroscopically (Pâris et al. 2017), has it been possible to construct a large sample of lensed quasars also in the optical (e.g. The Sloan Digital Sky Survey Quasar Lens Search, SQLS; Oguri et al. 2006), beyond the bright lenses identified in older searches.

More recently, thanks to new imaging sky surveys, with wide footprints and sufficient depth and image quality, like ATLAS

(Shanks et al. 2015), DES (The Dark Energy Survey Collaboration 2005; The Dark Energy Survey Collaboration et al. 2016), and KiDS (de Jong et al. 2015, 2017), the search for lensed quasars has received new impetus. Nevertheless, to this day, a big portion of the Southern Sky still remains unexplored and the spatial density on sky of known lenses remains much higher at Dec. > 0.

In order to fully exploit the wealth of data from different surveys, a suite of new methods to search for lensed quasars (QSOs) have been developed, based on morphology and visual inspection (Diehl et al. 2017; Lin et al. 2017); spectroscopy (e.g. Oguri et al. 2006; Inada et al. 2012; More et al. 2016); data mining on catalogue magnitudes (Agnello et al. 2015a; Agnello 2017; Williams, Agnello & Treu 2017); and variability (Berghea et al. 2017).

As recently quantified by Spiniello et al. (2018), different search methods are somewhat complementary, as each search relies on different criteria and ancillary information. The application of multiple, state-of-the-art methods over the same footprint then serves two scopes: assessing the role of selection bias in lens samples; and maximizing purity and completeness in lens searches.

With this paper, we perform a comparison study over the footprint covered by the Dark Energy Survey (DES) DR1 (The Dark Energy Survey Collaboration et al. 2016; Abbott et al. 2018), and present new lens candidates. Our choice is motivated by three criteria: the DES-DR1 release is public, which ensures reproducibility; its footprint lies mostly in the South, which is still largely unexplored;

★ E-mail: adriagnello@gmail.com
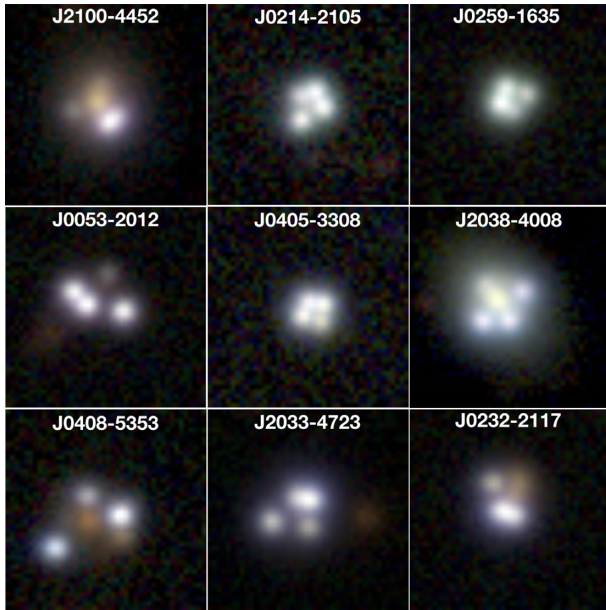
Figure 1. The nine quadruplets found by at least one method in the DES public footprint, with *WISE* extragalactic colours. The 11.5 arcsec × 11.5 arcsec cut-outs are obtained from the DES Data Access page, and are shown in DES *gri* bands. WG 2100-4452 is a previously unknown quad, and the discovery of WG 0214-2105 has been recently reported by Agnello (2018, RNAAS). WG J0053-2012 and WG 0405-33 have been found independently in STRIDES (Anguita et al. 2018; Schechter & Treu, private communication). Table 1 gives references for all quadruplets.

and the sheer convenience of display from the NCSA DESaccess cut-out service,[1] which enabled a swift visual inspection of image cut-outs. Magnitudes *W*1, *W*2, *W*3 from the *Wide-field Infrared Survey Explorer* (hereafter *WISE*; Wright et al. 2010) and from the *Gaia* space mission (Gaia Collaboration et al. 2016) are given in their native Vega system.

The paper is organized as follows. In Section 2, we describe each of the search methods, and its possible biases. In Section 3, we estimate the performance of each method, in terms of known lens recovery and of new candidates produced over the DES-DR1 footprint. We also provide tables of candidates, to facilitate spectroscopic follow-up, including at least two 'new' quadruplets: WG 210014.9-445206.4 and WG 021416.37-210535.3 (Fig. 1). We conclude in Section 4.

2 THE METHODS

We use five different methods, of which two are mostly morphological and rely on *Gaia* multiplet detection or chromatic offsets; one is based on spectroscopic pre-selection from fibre-spectroscopic surveys; and two are based on radio and X-ray pre-selection

The searches are structured similarly: a first step of *object pre-selection*, based on shallow cuts on catalogue magnitudes and colours; a second step of *target* selection, still based on catalogue entries; and a final step of *candidate* selection, through visual inspection of image cut-outs. For the sake of convenience, the DES-DR1 public cut-out service was used. However, in its current version, it properly displays between 50 per cent and 70 per cent

---

of the cut-outs that are produced due to software issues.[2] For this reason, the final numbers of candidates given in this paper should be taken as purely indicative, and a significant number of quasar lenses may still be found among the systems that were not properly displayed.

In what follows, the general performance on known systems is evaluated using a *benchmark* list of 214 known quasar lenses and pairs, collated from the CASTLES and SQLS (Inada et al. 2012) data bases, consistently with previous work (Williams et al. 2017). When restricting to the DES footprint, we will also consider lenses that have been found more recently through different endeavours (see Table 1).

2.1 BaROQuES: blue and red offsets of quasars and extragalactic sources

Here, we exploit observations of the same objects across different surveys, under the hypothesis that lenses can show astrometric offsets (across surveys with different waveband coverage, or depth, or image quality) due to the presence of different components. This enables a catalogue-based selection of composite objects regardless of blending issues, before examining the image cutouts.

The *Gaia* mission had ≈2 arcsec image resolution in DR1 and ≈0.5 arcsec in DR2, which enables the recognition of multiple images in lensed quasars that are otherwise not deblended by the image-processing pipelines of ground-based surveys. The search of quasar lenses in DES through *Gaia*-DR1 multiplet recognition has already been made within STRIDES (Agnello et al. 2018a). However, not all known lenses are deblended into multiple `source` entries in *Gaia*-DR1 (e.g. Agnello et al. 2018a). For this reason, we need complementary techniques to cope with incomplete deblending, in order to maximize completeness on lens searches.

For systems that are not *Gaia* multiplets, we can still use the accurate astrometry of *Gaia* to compare shifts in image centroids among different surveys. To this aim, we consider objects that are bright enough to have positions in the 2-Micron All-Sky Survey (2MASS) catalogue, and consider their 2MASS-*Gaia* offsets. Matters are slightly complicated, due to atmospheric differential refraction (ADR) and the choice of astrometric calibrators for each survey. Recent searches based on chromatic offsets (Lemon et al. 2017) relied on SDSS-versus-*Gaia* solutions, calibrated on astrometric reference stars, and had abundant contamination from isolated (unlensed) quasars. This is due to the different colours of quasars and astrometric stars, which can result in ≈0.3 arcsec offsets due to ADR (with typical ≈20 deg zenith angles of ground-based surveys).

We resolve this by means of field-corrected offsets, using our own BaROQuES scripts,[3] as follows. First, we work with a sample of quasar-like objects, selected in *WISE* as[4]

$$W1 - W2 > 0.35 - \sqrt{(\delta W1)^2 + (\delta W2)^2}, \tag{1}$$

$$W1 - W2 > 0.2 + \sqrt{(\delta W1)^2 + (\delta W2)^2}, \tag{2}$$

---

[2]We did not contact the NCSA helpdesk immediately and directly to address this problem, and we still do not understand its cause. However, the main results in this paper are unaffected.

[3]Blue and Red Offsets of Quasars and Extragalactic Sources, available upon request, https://github.com/aagnello.

[4]The *WISE* magnitudes include light from a blend of components, due to its FWHM ≈ 6 arcsec image resolution.

[1]https://des.ncsa.illinois.edu/easyweb

Table 1. Known lenses in the DES-DR1 public footprint recovered by the different search methods of Section 2. Magnitudes are from *WISE* and *Gaia*-DR1 and given in the Vega system. The first six systems in the table are the known quadruplets, whose cut-outs are also shown in Fig. 1. Here, W2MG1 denotes 2MASS-versus-*Gaia* chromatic offsets (see Section 2.1), and 'mult' or 'sing' marks objects that correspond to *Gaia* multiplets or singlets, respectively.

object	W1	W2	W3	G	Methods	Reference
J005344.44−201233.7	14.56 ± 0.03	14.01 ± 0.04	10.76 ± 0.10	19.21	GaiaDR2mult	STRIDES (in preparation)
J021416.37−210535.3	15.11 ± 0.03	14.68 ± 0.06	11.82 ± 0.24	19.80	GaiaDR2mult	Agnello (2018, RNAAS)
J023233.16−211725.7	14.02 ± 0.03	12.99 ± 0.03	10.06 ± 0.05	18.93	XMMslew	Wisotzki et al. (1999)
J025942.86−163543.0	13.86 ± 0.03	13.13 ± 0.03	10.03 ± 0.05	19.22	W2MG1sing	Schechter et al. (2018)
J040559.76−330851.0	13.85 ± 0.03	12.71 ± 0.02	9.94 ± 0.04	20.22	W2MG1mult, GaiaDR2mult	Anguita et al. (2018)
J040821.63−535358.9	14.08 ± 0.02	13.17 ± 0.02	10.75 ± 0.06	19.63	GaiaDR2mult	Lin et al. (2017)
J203342.12−472343.9	13.49 ± 0.03	12.34 ± 0.03	9.25 ± 0.04	17.98	W2MG1mult, GaiaDR2mult	Morgan et al. (2004)
J203802.69−400813.9	11.43 ± 0.02	10.25 ± 0.02	7.49 ± 0.02	19.44	W2MG1mult, GaiaDR2mult, 6dFGS	Agnello et al. (2018a)
J011557.37−524423.4	14.49 ± 0.03	13.36 ± 0.03	10.82 ± 0.11	20.40	GaiaDR2mult	Agnello et al. (2015b)
J014632.87−113339.2	14.17 ± 0.03	13.08 ± 0.03	10.45 ± 0.06	18.39	W2MG1mult, GaiaDR2mult	Agnello et al. (2018a)
J023527.42−243313.8	14.00 ± 0.03	13.02 ± 0.03	10.29 ± 0.05	18.12	W2MG1mult, GaiaDR2mult	Agnello et al. (2018a)
J051410.90−332622.4	13.29 ± 0.03	11.71 ± 0.02	8.54 ± 0.02	17.80	HE, RASS	Gregg et al. (2000)
J202139.38−411557.9	14.17 ± 0.03	13.17 ± 0.03	10.44 ± 0.07	19.27	W2MG1mult, GaiaDR2mult	Agnello et al. (2018a)

$$W2 - W3 > 2.1 + \sqrt{(\delta W2)^2 + (\delta W3)^2}, \tag{3}$$

$$W1 < 17, W2 < 15.6, W3 < 11.8. \tag{4}$$

Then, for each given object we examine a surrounding patch of 1.0×1.0 deg^2, containing ≈ 40 QSO-like neighbours. We then compute the average offsets between their 2MASS and *Gaia* coordinates $\delta x = -\cos(\text{Dec.})\delta$RA, $\delta y = \delta$Dec., subtract them from the offsets of the given object, and retain it only if this corrected offset is between 0.27 and 1.8 arcsec. This ensures that known lenses are recovered, and chance alignments of quasars with other objects are safely rejected. The lower threshold in separation is chosen because the root-mean-square (field-corrected) offsets of isolated objects can be up to 0.2–0.3 arcsec in each patch.

When applied to the Southern Galactic hemisphere, with $b < -20$ and $-70 < $ Dec. < 7, this gave $\approx 6 \times 10^4$ objects, of which 31 381 singlets and 770 multiplets in the DES-DR1 footprint.

2.2 *Gaia*-DR2 multiplets

The nominal resolution of *Gaia* has improved from 2 arcsec (DR1) to 0.4 arcsec (DR2), so a simple upgrade consists in searching again for *Gaia*-DR2 multiplets corresponding to *WISE* sources. There is indeed some improvement from DR1 to DR2: out of the $\approx 6 \times 10^4$ *Gaia*-DR1 singlet 'BaROQuES' from above, a match with DR2 gave 2149 multiplets, of which 134 with more than two `source` entries.

However, some candidates and small-separation lenses from DR1 have disappeared in the passage to DR2 (e.g. WGD0508; Agnello et al. 2018a). The same has been noticed by Spiniello et al. (2018) on a smaller footprint (KiDS-DR3, 450 deg^2). In general, the *Gaia*-specific deblending does not seem to have a well-defined behaviour with separation and flux ratios, as some small-separation lenses are recognized as multiplets while larger-separation lenses correspond to *Gaia* singlets (e.g. WGD0150, WGD0245; Agnello et al. 2018a).

In order to make additional progress over the searches in *Gaia*-DR1, we also relaxed the pre-selection photometric criteria. From a *WISE* search, we selected extragalactic objects as

$$W1 - W2 > 0.2 + \sqrt{(\delta W1)^2 + (\delta W2)^2}, \tag{5}$$

$$W1 < 17, W3 < 12.4 \tag{6}$$

basically excluding stars ($W1 - W2 \approx 0$) and fainter objects with unreliable catalogue magnitudes. This gave $\mathcal{O}(10^6)$ objects with Galactic latitude $b < -15$. Of these, $\mathcal{O}(10^5)$ are recognized as multiplets in *Gaia*-DR2.[5] However, many are clustered towards the Galactic disc and the Magellanic Clouds, which can be explained with the line-of-sight alignment of quasars with stars. In order to exclude most quasar-star pair contaminants, we then impose a threshold on the ratio Σ_m/Σ_s, between densities of multiplets (Σ_m) and singlets (Σ_s), estimated in 0.5×0.5 deg^2 patches around each multiplet.[6] For the *Gaia* doubles, we retain only objects in regions where $\Sigma_m/\Sigma_s < 0.2$; for *Gaia* triplets and quadruplets, we relax it to $\Sigma_m/\Sigma_s < 0.3$. After the overdensity threshold cuts, $\approx 17\,000$ multiplets remain, of which 8146 lie in the DES-DR1 public footprint.

2.3 Spectroscopic surveys

Some of the longest known quasar lenses, such as e.g. Q0957+561 (Walsh, Carswell & Weymann 1979) and lenses from the Hamburg-ESO survey (Wisotzki et al. 1996), were found in wide-field, prism spectroscopic surveys. Over the last decade, searches in the SDSS and BOSS (Inada et al. 2012; More et al. 2016) relied on samples of objects that were classified as quasar based on fibre spectroscopy. Also, some lenses recently found in the DES (Ostrovski et al. 2017; Agnello et al. 2018a) had pre-existing fibre spectra in the Anglo-Australian Observatory data bases, where they had been targeted as quasars or galaxies and not recognized as lenses, due to low image resolution.

For this reason, we examined two surveys with moderate depth and uniform coverage over large areas in the Southern hemisphere: the six-degree field galaxy survey (6dFGS; Jones et al. 2004) and the 2QZ (Boyle et al. 2000). These two surveys were also based on different pre-selection cuts, based on optical cuts in all-sky surveys of moderate depth, focusing on galaxy-like (6dFGS) or quasar-like

---

[5]Matching radius of 5 arcsec; Spiniello et al. (2018) have checked the validity of this choice.
[6]See also Agnello (2018, RNAAS).

(2QZ) objects. In this sense, then, they are also complementary to the *WISE* criteria that we have used in our photometric searches.

We restrict these samples to objects with[7] *pipeline redshifts* $z_s > 0.5$, as expected from simulated samples (OM10) and our benchmark of CASTLES/SQLS known lenses. This gave 1625 objects from the 6dFGS and 7147 from 2QZ, over the DES footprint. Due to the different choices in optical colour pre-selection of the 6dFGS and 2QZ, there is no overlap between the candidate samples from these two surveys.

2.4 X-Ray

Quasars can also be identified by X-ray emission, due to lower dust attenuation in that spectral range. The recently vetted cross-match (Salvato et al. 2018) the *ROSAT* all-sky survey (Boller et al. 2016) and XMMslew survey (Georgakakis & Nandra 2011) with *WISE* then provides an alternative pre-selection of possible candidates. Some lenses discovered in *ROSAT* are indeed known, such as RXJ0911.4+0551 (Bade et al. 1997), RXJ0921+4529 (Muñoz et al. 2001), and RXJ1131−1231 (Sluse et al. 2003). A fainter lens, CY2201−3201 (Castander et al. 2006) was found in the *Chandra* deep fields.

We then used the publicly available cross-match tables[8] to preselect X-ray objects. Also in this search, we excluded possible stars with the same cuts as above (equations 5 and 6). This yielded 13 547 cut-outs from *ROSAT–WISE* and 2294 from *XMM–WISE*.

2.5 Radio

Similarly to X-ray pre-selection, radio searches are less affected by reddening and by the presence of a foreground galaxy. As a consequence, they bypass the colour selection that can affect optical or IR searches. Indeed, quasar lens discoveries in the past have benefited from hemispheric surveys like the Parkes-MIT-NRAO survey (Griffith & Wright 1993) and dedicated observations by the CLASS (Myers et al. 2003) and J-VLA (King et al. 1999) searches.

Here, we use the Sydney University Molonglo Sky Survey (SUMSS; Mauch et al. 2003), covering the Southern hemisphere down to ≈10 mJy at 0.84 GHz. We match the catalogue with *WISE*, using a nearest-neighbour match with 10 arcsec search radius, and retained extragalactic objects as above (equations 5 and 6). This resulted in 38 204 cut-outs within the DES-DR1 footprint.

3 PERFORMANCE AND RESULTS

The performance of each method can be quantified in different ways. One metric is given by completeness and purity with respect to previous searches. Another possibility is the number of candidates that are produced by each method over the same footprint. The final evaluation of performance is the purity of the candidate samples, once spectroscopic follow-up is performed. Most of the candidates presented in this paper are still awaiting spectroscopic confirmation, and published samples of lenses and contaminants over the DES footprint are still too small to build robust statistics. Then for the scope of this paper, we discuss the recovery of known lenses over DES-DR1, and properties of candidate samples from different searches. We also provide estimates of completeness and purity,

based on the expected fraction of quadruplets. These are in line with findings of ongoing spectroscopic campaigns (Spiniello et al. 2019).

3.1 Known lenses and the DES subsample

Table 1 lists the known lenses recovered over the DES-DR1 footprint. Five lenses are two image systems, and eight are (at least) quadruplets. Two of them (WG 0405-3308 and WG 0053-2012) have also been found, independently, within the STRIDES collaboration (Anguita et al. 2018; Schechter & Treu, private communication). The discovery of WG 0214-2105 has been recently reported by Agnello (2018). The two 'new' quad candidates, WG 2100-4452 and WG 0214-2105, have just recently been confirmed spectroscopically, and have been shown to be well reproducible by simple lens models (Wynne & Schechter 2018).

The recovery statistics of known lenses in *Gaia*-DR2 is slightly better than for *Gaia*-DR1 (e.g. Agnello 2018). We quantify this through the *benchmark* list of 214 CASTLES/SQLS systems introduced in Section 2. Of these, 43 are missing from *Gaia*-DR2. Of the 171 that are detected, 124 are resolved in two sources, 15 into three sources, and 6 into four sources. Small-separation lenses are absent in *Gaia*-DR2, because of a sharper cut-off at ≈0.5 arcsec separations in the DR2 catalogue. These include also systems that were found thanks to *Gaia*-DR1 (e.g. WGD 0508; Agnello et al. 2018b).

3.2 Candidates

Visual inspection of targets from the above methods resulted in 16 BaROQuES in *Gaia*-DR1 versus 2MASS (not counting WG0214, already reported, see Table 1), of which 5 *Gaia* multiplets; 20 candidates from *Gaia*-DR2 multiplets (including WG2100, reported here for the first time); 7 candidates from fibre-spectroscopy (3 from 6dFGS and 4 from 2QZ); 29 candidates from X-ray pre-selection, of which 28 from *ROSAT*; and 26 candidates from SUMSS. The full lists of high-graded candidates are provided in Tables A1 and A2, divided by search method. We list their names (J2000 coordinates), as well as their *WISE* (*W*1, *W*2, *W*3) and *Gaia*-DR1 (*G*) magnitudes. These total to 98 unique candidates.

The number of targets and candidates per square degree from each search depends on its depth and design. Searches relying on SUMSS, *ROSAT*, 2MASS, and *Gaia* resulted in comparable numbers of candidates (modulo the depth limits of each survey). The search based on the 6dFGS, while nominally using a hemispheric survey, resulted in much fewer candidates, because the catalogue objects themselves had been selected as nearby galaxy candidates based on their optical colours.

Fig. 2 shows the colour and magnitude distributions of the candidates. Different colours and markers represent the different methods through which the candidates have been identified. Known lenses are plotted in red (dashed in the magnitude histograms, triangles in the colour–colour plot). *Gaia*-selected candidates extend the regime of known lenses towards fainter magnitudes, still with a cut-off at the faint end due to noisy *WISE* magnitudes and the drop in *Gaia* completeness at $G \approx 20$. X-ray and radio-selected candidates populate the faint end of the magnitude distribution, with few objects corresponding to optical detections in *Gaia* (26 of these objects are missed by *Gaia* DR1 and/or DR2).

Two main clusters of systems are visible in the *WISE* colour–colour plot: objects with high $W1 - W2$, compatible with QSO-dominated photometry, and systems with lower $W1 - W2$, compatible with galaxy-dominated photometry. Systems with low $W1 -$

---

[7]The public releases of 6dFGS and 2QZ provide a redshift for each object, determined through automated pipelines.
[8]http://www.mpe.mpg.de/XraySurveys/2RXS/
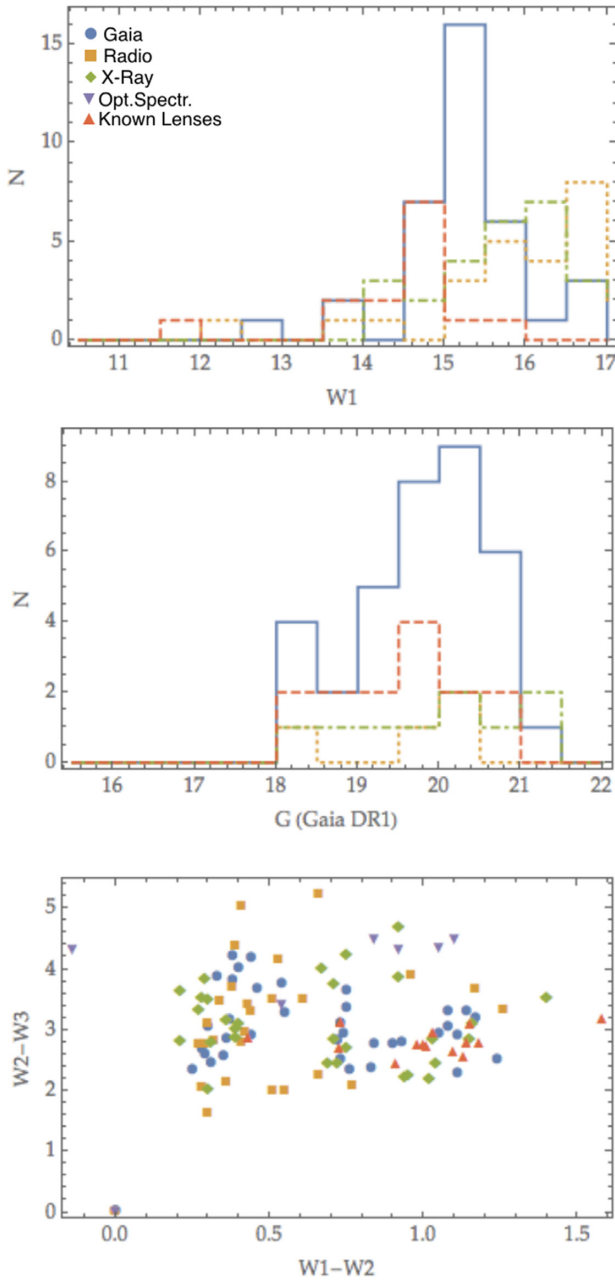
Figure 2. Magnitude and colour distributions of candidates and known lenses. *Left: W1 −* magnitude distribution for *Gaia* candidates (blue), radio candidates (orange, dotted), X-ray candidates (green, dot–dashed) and known lenses (red, dashed), truncated to the *WISE* completeness limit $W1 = 17$. *Middle: G −*magnitude distribution, with the same colour coding. *Right:* colours $W1 − W2$ versus $W2 − W3$, same colour coding (and markers) as in the first panel. We have added WG 2100-4452 to the sample of 'known' quadruplets, instead of showing it separately. BaROQueS and Multiplets are grouped, because they are based on *Gaia*. Red triangles represent the known lenses recovered by the five searches.

$W2$ (left-most panel) mostly have $W3 \geq 11.8$, which is the threshold where *WISE* magnitudes become unreliable. There is a prevalence of radio-selected objects in the galaxy-dominated clump, whereas X-ray and *Gaia*-selected systems are evenly distributed. Known lenses are mostly associated with the QSO-dominated regime.

Candidates selected from each method are shown in Figs 3 and 4. All methods produce sensible results upon visual inspection, albeit

with a pre-dominance of high-grade candidates from the *Gaia* searches. Some candidates (mostly from SUMMS and spectroscopic surveys) may be lenses with bright deflectors, or mergers of compact narrow-line galaxies at lower redshift. With the depth ($i \approx 22.5$) and image resolution of Pan-STARRS and DES-DR1 (≈ 0.26 arcsec pixel^{-1}, ≈ 1 arcsec seeing), these contaminants are still present in candidate samples.

Visual inspection is a critical step in candidate selection. Quadruplets are often clear to recognize, especially after some simple, model-based scoring (e.g. Wynne & Schechter 2018). Doubles, on the other hand, are less obvious: contaminants include physical or line-of-sight pairs of quasars; line-of-sight pairs of quasars and stars or galaxies; pairs of compact narrow-line galaxies; and galaxies seen through two stars. Some *nearly identical* quasar pairs (or NIQs; Agnello et al. 2018a) may actually be lenses whose deflector is too faint to be detected in ground-based discovery data, especially at small separations (as discussed e.g. by Morgan et al. 2000). High-grade candidate doubles were then selected based on whether the putative quasar images had same colours, and whether a candidate deflector galaxy was visible in between, for image-separations larger than ≈ 1.5 times the seeing.

3.3 Quadruplets

Due to their higher number of images, with respect to doubles, quadruplets yield more constraints on the deflector potential and stellar mass fraction, and for this reason, they are especially valued probes of cosmography (e.g. Refsdal 1964; Blandford & Narayan 1992; Witt, Mao & Keeton 2000; Suyu et al. 2013; Treu & Marshall 2016; Bonvin et al. 2017) and microlensing studies (e.g. Schechter et al. 2014).

A quadruplet configuration requires an even closer alignment of source and deflector than doubles. The fraction of quadruplets in statistically complete quasar lens samples is estimated at 14 per cent (OM10). The two quadruplets found within this search, WG 210014.9-445206.4 and WG 021416.37-210535.3, correspond to *Gaia*-DR2 triplets and are already shown in Fig. 1. Most of the other candidates, except some radio-selected and spectroscopically selected candidates, are doubles. We emphasize that, while WG 0214-2105 requires little follow-up for confirmation, in principle the chromaticity in WG 2100-4452 requires a final step of spectroscopic confirmation to secure its lensing nature.[9] Still, both have been shown to be easily compatible with simple lens models (Wynne & Schechter 2018).

Two other quadruplets found in this search, at J0405−3308 and J0053−2012, have also been discovered independently within the STRIDES[10] collaboration (Schechter & Treu, private communication). Even though they were found *blindly* by our search, using exclusively public data sets, and so would be legitimate candidates in the framework of this paper, we prefer to list them as known lenses (Anguita et al. 2018; STRIDES in preparation).

3.4 Completeness and purity

The statistics of quadruplets is also an indication of completeness in a quasar lens search, relative to the number of objects at pre-selection. One could also use two-image lenses for the same

---

[9]After this paper was submitted, this lens was confirmed with $z_s \approx 3.1$ (Anguita & Schechter, private communication).
[10]STRIDES is a broad external collaboration of the DES, strides.astro.ucla.edu.

W2MG1
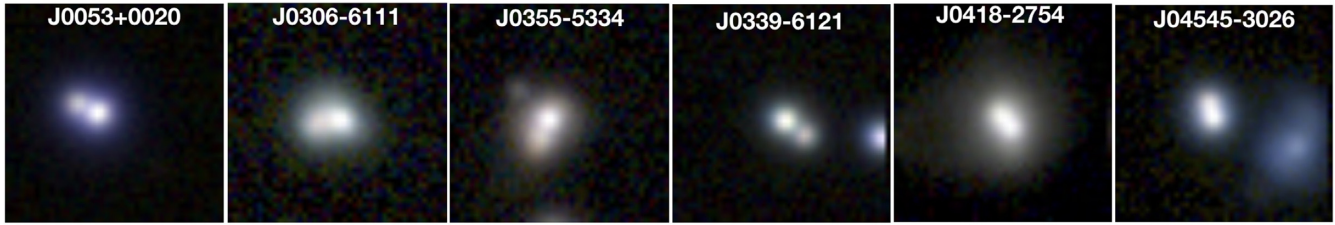
GaiaDR2-Multiplets

Figure 3. Examples of candidates found in *Gaia* DR1 and DR2, with *WISE* pre-selection (same colour scheme as in Fig. 1). W2MG1 denotes *WISE* objects with acceptable offsets between their 2MASS and *Gaia*-DR1 catalogue positions, with recomputed astrometry from our BaROQuES scripts.

computation, but those generally require extensive campaigns of spectroscopic confirmation, whereas quadruplets are almost unmistakeable already from photometry and simple modelling (as e.g. by Wynne & Schechter 2018). What follows is a simple check based on OM10 as reanalysed by Treu et al. (2018) and more agnostic estimates (i.e. independent of OM10) from known lenses in the smaller footprint of KiDS ($\approx$450 deg^2) by Spiniello et al. (2018).

A 'demanding' quasar pre-selection (e.g. $W1 - W2 > 0.55 + \sqrt{(\delta W1)^2 + (\delta W2)^2}$; Agnello et al. 2018b) produces $\approx$40 objects per square degree, which (adopting OM10 lensing rates) gives $\approx$20 lenses over the DES footprint, of which $\approx$2.8 $\pm$ 1.67 should be quads. A *WISE* pre-selection like the ones in this paper produces 110 $\pm$ 10 objects per square degree, and should result in 7.7 $\pm$ 0.7 quadruplets over the DES footprint.

The numbers given above, however, adopt a rough OM10 estimate that may simply be unreliable. In fact, the lensing rate of quasars is not a direct measurement of those that can actually be detected or recognized, due e.g. to the image quality of a survey or the relative importance of fluxes from quasar images and deflector galaxies. Treu et al. (2018) have compared a mock sample of lensed quasars, built along the lines of OM10 and rendered into the imaging specifics of the DES, and found that the estimated rates agree with the currently known lenses (including some reported in this paper) only at the bright end ($i \lesssim$ 18.1), and many lenses predicted by OM10+DES were probably undiscovered at fainter magnitudes. On the other hand, Spiniello et al. (2018) have found that there are at least 9 quasar lenses in the KiDS-450 footprint, whereas the same

OM10 estimates would have predicted 6. Therefore, the expected number of lenses (including quadruplets) should be $\approx$1.5 times higher, predicting $\approx$12 quadruplets in the DES footprint from our pre-selection criteria.

For the searches in this paper, the lensing rates should also be multiplied by the $\approx$0.6 success rate by which the NCSA cut-out server correctly displayed images,[11] yielding again $\approx$7 quadruplets over the DES from our choices of pre-selection – or 5–10, adopting simplistic Poissonian statistics and fluctuations in the NCSA cut-out display success rate. Then, the 9 quadruplets (discovered or recovered) in this paper suggest that the steps of target and candidate selection are reasonably complete.

In order to find more quads, then, the main bottleneck is that of colour pre-selection. Searches with hybrid, optical–IR colours would allow one to relax the *WISE* extragalactic cuts, but in this exploration, we preferred to use the DES-DR1 only for the final stage of visual inspection in order not to impose a prejudice on the optical colours of lensed quasars upon our searches.

The number of quadruplets also indicated the expected purity of the whole candidate sample. With the figures above, we would expect $\approx$60 candidate doubles to actually be lenses. The current sample of $\approx$100 candidates then suggests a purity of $\approx$60 per cent. The success rate of ongoing spectroscopic campaigns (Spiniello et al. 2019) confirms this estimate.

---

[11] Again, we should stress that this refers to when these searches were performed and to the current version of this paper.

RASS
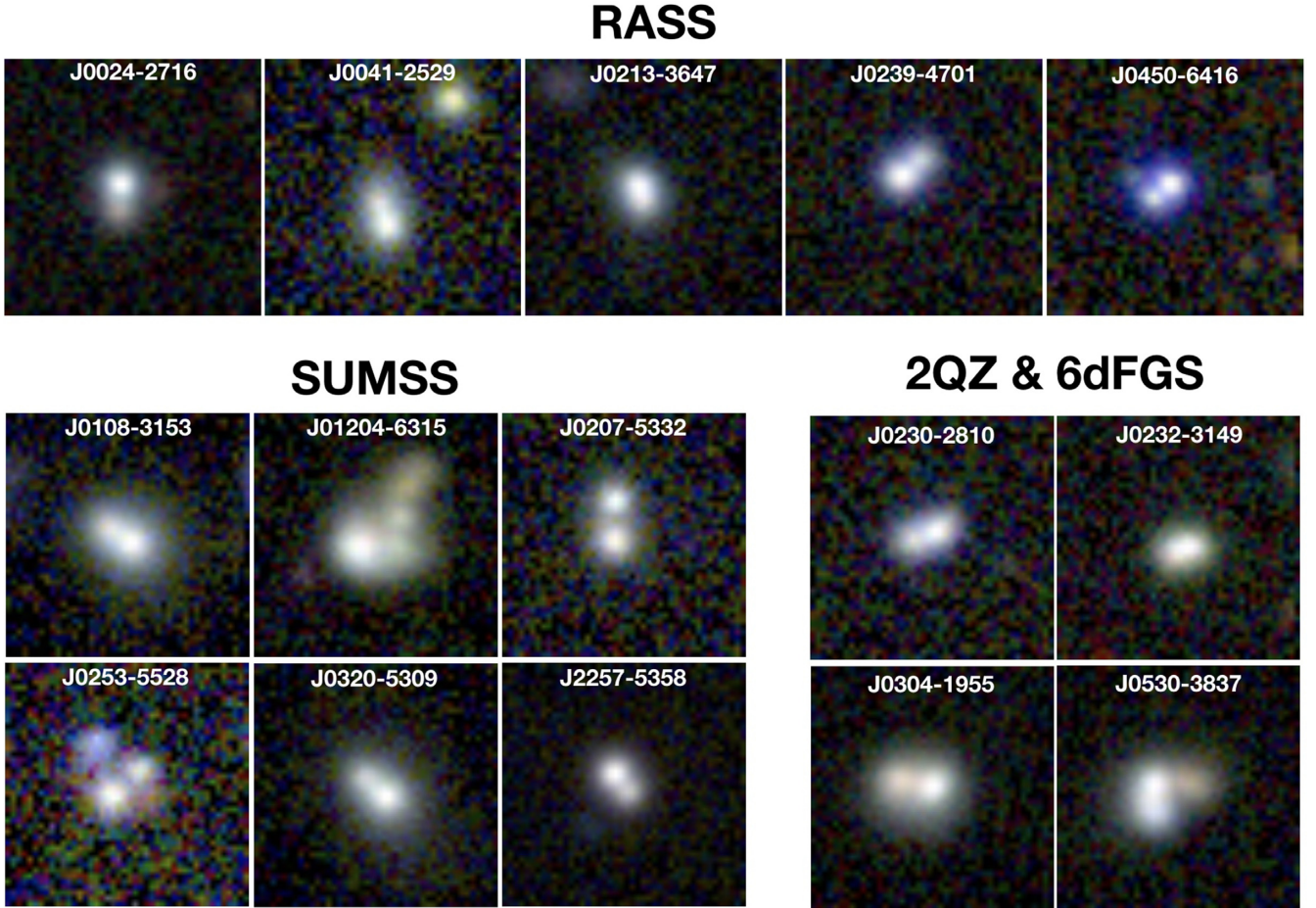
SUMSS

2QZ & 6dFGS

Figure 4. Examples of candidates found with spectroscopic (2QZ, 6dFGS), radio (SUMMS), or X-ray (*ROSAT*, XMMslew) surveys.

4 DISCUSSION

We have discovered two previously unknown quadruplets, WG210014.9-445206.4 and WG021416.37-210535.3. We have independently discovered another two (J0053−2012, J0405−3308) found independently within STRIDES (Anguita et al. 2018; STRIDES in preparation), which we prefer to list among other known lenses in the DES footprint.

The use of five different selection methods, over spectral ranges ranging from X-ray to radio through optical, has resulted in 100 quasar lens candidates over the DES-DR1 public footprint. The number of quadruplets found in this paper suggests that the searches are reasonably complete and that the main bottleneck is the very first step of object pre-selection

All of the searches involved a step of *WISE* pre-selection, imposing some loose cuts on colours in order to isolate extragalactic objects, and results in two main clusters of candidates based on whether their photometry is quasar dominated or galaxy dominated. Due to the capabilities of the DESaccess server with large cut-out queries, at least at the time when these searches were performed, approximately two-thirds of targets in the DES-DR1 footprint were properly displayed, so another ≈50 candidates may be still awaiting discovery.

The depth of lens searches is still an open issue. Despite the nominal depth ($i \approx 22.5$) of the DES public data, current campaigns over the DES footprint are covering the brighter end ($i \lesssim 18.5$, as shown by Treu et al. 2018; Spiniello et al. 2019). This is partly due to the completeness limit of *Gaia*, and the need to identify promising candidates upon visual inspection. From the searches in this paper, a pre-selection-based e.g. radio or X-ray emission seems to aid the identification of lens candidates at fainter (optical and IR) magnitudes than has been possible so far (see Fig. 2).

4.1 Deeper and sharper *WISE* pre-selection

At the stage of *WISE* pre-selection, we are currently limited by two factors: the uncertainties in $W1$, $W2$, $W3$ magnitudes; and image resolution. First, the searches are cut at $W1 < 17$ and $W2 < 15.6$, since the magnitudes of fainter objects are more affected by Earth-shine and become quickly unreliable. Secondly, the ≈6 arcsec (full width at half-maximum, FWHM) image resolution of *WISE* prevents any comparison of the mid-IR colours of different components, which at these wavelengths should be unaffected by reddening and microlensing and would then make a powerful selection criterion.

Forced photometry upon *WISE* cut-outs, using object positions from sharper surveys (like Gaia or the DES), would alleviate these issues and enable a deeper and sharper search, maximizing the information content of *WISE*. This, of course, requires that multiple components are identified by the optical surveys and that their separation is wide enough ($\gtrsim 2.5$ arcsec) so that the magnitudes inferred through forced photometry are reliable. From a re-reduction

(Meisner, Lang & Schlegel 2017) and forward modelling of *WISE*/Neo*WISE* survey tiles, forced-photometry magnitudes are currently available for the SDSS (Lang, Hogg & Schlegel 2016) and the DECaLS (Dey et al. 2019) footprints, covering 'Northern' declinations above −20 deg. By using *Gaia* multiplets as a base for forced photometry, a search based on mid-IR (deblended) colours may be extended to the whole sky. However, the completeness of the resulting sample would be ill characterized, as the current releases of *Gaia* fail to properly deblend lenses (e.g. WGD 0150, WGD 0245, Agnello 2017) that are clearly deblended into multiplets by other surveys such as the DES.

Another way of increasing depth and imaging resolution, in the BaROQuES approach, would be to replace 2MASS with deeper surveys, such as UKIDSS (Warren et al. 2007) or VHS (McMahon et al. 2013). However, their sky coverage is not homogeneous, whereas 2MASS covers the whole sky, and their application to a DES search is of limited use since their overlap with the DES footprint is only partial. Wile UKIDDS is primarily a Northern hemisphere survey, VHS was planned to cover the whole Southern hemisphere, but[12] it is mostly limited to −20 ≤ Dec. < 0 and −50 ≤ Dec. < −40, and not homogeneously.

4.2 Towards the LSST

While near-IR surveys (e.g. VHS, UKIDSS, and VHS) are ideally suited for chromatic offsets, due to the different colours of sources and deflectors, optical surveys can be a valid alternative. Lemon et al. (2018) have successfully used SDSS instead of 2MASS, and our BaROQuES procedures have been applied with success to the KiDS-DR3 450 deg^2 footprint (Spiniello et al. 2018). In the near future, LSST (SV due 2022, SciOps due 2023) will enable the extension of these searches to the whole Southern hemisphere.

Despite the deluge of multi-epoch data from the full survey, the foreseen volume of nightly observations is still manageable, and automated procedures for chromatic offsets can be run on a nightly basis. This pipeline-oriented approach will then bring the discovery of lensed quasars to the same, high-cadence pace of transient discoveries. Ideally, chromatic offsets can be computed among different bands within LSST, without the recourse to external surveys like *Gaia* or 2MASS, provided nightly data are deep enough to guarantee robust astrometry in separate bands.

4.3 *Gaia* DR3, DR4, and *Euclid*

The DR2 of *Gaia* provided additional information over DR1, such as blue and red pass-band magnitudes (G_{bp}, G_{rp}), as well as parallax and proper motion, for sources towards the bright end. It has a safety cut-off at ≈0.5 arcsec nearest neighbours, which prevents the discovery of small-separation lenses through multiplet recognition but may be reassessed in future releases. The pipeline proper motions of known lenses are not necessarily small (Spiniello et al. 2018), and colours from G_{bp}, G_{rp} can only be used for the brighter candidates.

The final *Gaia*-DR4 release, due in 2020, is planned to provide low-resolution spectra of all detected *Gaia* sources. This would provide a selection of lens candidates based uniquely on *Gaia*, bypassing broad-band colour selection, through the detection of

emission lines from the source quasars. This approach closely resembles the Hamburg-ESO strategy of isolating quasars based on their low-resolution spectra and following them up with higher imaging resolution, but it would be applied over the whole sky and down to fainter magnitudes.

Beyond the spectroscopic and multiplet selection in *Gaia*, an obvious step forward will be the Euclid space mission (Laureijs et al. 2010). The lessons learnt from the *Gaia* pipelines, in deblending objects into multiple sources and extracting spectra, will be essential to the development of lens searches within Euclid. In these all-sky perspectives, significant improvement is needed on the final stage of candidate selection, whether it is based on direct cutout modeling or direct visual inspection. Dedicated deblenders are being developed to this purpose (e.g. Chan et al. 2015; Schechter et al. 2018), but they still require manual 'tuning' to the specifics of each survey, and a considerable amount of visual inspection.

4.4 Beyond *ROSAT*: *eROSITA*

The optical and X-ray choices of pre-selection are quite complementary. On the one side, X-ray-selected sources populate the faint end of the *WISE* and *Gaia* magnitude distribution, and sometimes miss *Gaia* `source` counterparts. On the other, only two of the known lenses in the DES are detected by our *ROSAT–WISE* search, and in general X-ray-selected lenses are a minority among the CASTLES sample.

In the near future, *eROSITA* (Merloni et al. 2012) promises a ≈20 deeper coverage than *ROSAT* in the soft X-ray, and the first ever all-sky survey in the hard X-ray. The forecast of ≈100 detected objects per square degree, over the 4-yr span of the survey mission, is comparable to the *WISE* extragalactic selections used in this paper, and based on completely independent spectral signatures. In particular, from the expected number of active galactic nuclei (AGNs) with redshift $1 < z_s < 3$ and the OM10 estimates, *eROSITA* should detect ≈120 lensed quasars over its 30 000 deg^2 footprint, a quarter of which would have an obscured AGN as a source.

---

[12]Based on the final release (2018-02-09) by the ESO Archive Group, https://www.eso.org/qi/catalog/show/217, see 'Description' for warnings on catalogue usage and missing entries.

REFERENCES

Abbott T. M. C. et al., 2018, ApJS, 239, 18
Agnello A., 2017, MNRAS, 471, 2013
Agnello A., 2018, RNAAS, 2, 42
Agnello A., Kelly B. C., Treu T., Marshall P. J., 2015a, MNRAS, 448, 1446
Agnello A. et al., 2015b, MNRAS, 454, 1260
Agnello A. et al., 2018a, MNRAS, 475, 2086
Agnello A. et al., 2018b, MNRAS, 479, 4345
Anguita T. et al., 2018, MNRAS, 480, 5017
Bade N., Siebert J., Lopez S., Voges W., Reimers D., 1997, A&A, 317, L13
Berghea C. T., Nelson G. J., Rusu C. E., Keeton C. R., Dudik R. P., 2017, ApJ, 844, 90
Blandford R. D., Narayan R., 1992, ARA&A, 30, 311
Boller T., Freyberg M. J., Trümper J., Haberl F., Voges W., Nandra K., 2016, A&A, 588, A103
Bonvin V. et al., 2017, MNRAS, 465, 4914
Boyle B. J., Shanks T., Croom S. M., Smith R. J., Miller L., Loaring N., Heymans C., 2000, MNRAS, 317, 1014
Castander F. J., Treister E., Maza J., Gawiser E., 2006, ApJ, 652, 955
Chan J. H. H., Suyu S. H., Chueh T., More A., Marshall P. J., Coupon J., Oguri M., Price P., 2015, ApJ, 807, 138
Dark Energy Survey Collaboration et al., 2016, MNRAS, 460, 1270
de Jong J. T. A. et al., 2015, A&A, 582, A62
de Jong J. T. A. et al., 2017, A&A, 604, A134
Dey A. et al., 2019, AJ, 157, 168
Diehl H. T. et al., 2017, ApJS, 232, 15
Gaia Collaboration et al., 2016, A&A, 595, A1
Georgakakis A., Nandra K., 2011, MNRAS, 414, 992
Griffith M. R., Wright A. E., 1993, AJ, 105, 1666
Gregg M. D., Wisotzki L., Becker R. H., Maza J., Schechter P. L., White R. L., Brotherton M. S., Winn J. N., 2000, AJ, 119, 2535

Inada N. et al., 2012, AJ, 143, 119
Jones D. H. et al., 2004, MNRAS, 355, 747
King L. J., Browne I. W. A., Marlow D. R., Patnaik A. R., Wilkinson P. N., 1999, MNRAS, 307, 225
Lang D., Hogg D. W., Schlegel D. J., 2016, AJ, 151, 36
Laureijs R. J., Duvet L., Escudero Sanz I., Gondoin P., Lumb D. H., Oosterbroek T., Saavedra Criado G., 2010, Proc. SPIE, 7731, 77311H
Lemon C. A., Auger M. W., McMahon R. G., Koposov S. E., 2017, MNRAS, 472, 5023
Lemon C. A., Auger M. W., McMahon R. G., Ostrovski F., 2018, MNRAS, 479, 5060
Lin H. et al., 2017, ApJ, 838, L15
Mauch T., Murphy T., Buttery H. J., Curran J., Hunstead R. W., Piestrzynski B., Robertson J. G., Sadler E. M., 2003, MNRAS, 342, 1117
McMahon R. G., Banerji M., Gonzalez E., Koposov S. E., Bejar V. J., Lodieu N., Rebolo R., VHS Collaboration 2013, Messenger, 154, 35
Meisner A. M., Lang D., Schlegel D. J., 2017, AJ, 154, 161
Merloni A. et al., 2012, preprint (arXiv:1209.3114)
More A. et al., 2016, MNRAS, 456, 1595
Morgan N. D. et al., 2000, AJ, 119, 1083
Morgan N. D., Caldwell J. A. R., Schechter P. L., Dressler A., Egami E., Rix H.-W., 2004, AJ, 127, 2617
Muñoz J. A. et al., 2001, ApJ, 546, 769
Muñoz J. A., Falco E. E., Kochanek C. S., Lehár J., Mediavilla E., 2003, ApJ, 594, 684
Myers S. T. et al., 2003, MNRAS, 341, 1
Oguri M., Marshall P. J., 2010, MNRAS, 405, 2579 (OM10)
Oguri M. et al., 2006, AJ, 132, 999
Ostrovski F. et al., 2017, MNRAS, 465, 4325
Pâris I. et al., 2017, A&A, 613, A51
Refsdal S., 1964, MNRAS, 128, 307
Salvato M. et al., 2018, MNRAS, 473, 4937
Schechter P. L., Pooley D., Blackburne J. A., Wambsganss J., 2014, ApJ, 793, 96
Schechter P. L., Anguita T., Morgan N. D., Read M., Shanks T., 2018, RNAAS, 2, 21
Shanks T. et al., 2015, MNRAS, 451, 4238
Sluse D. et al., 2003, A&A, 406, L43
Spiniello C. et al., 2018, MNRAS, 480, 1163
Spiniello C., Agnello A., Sergeyev A. V., Anguita T., Rodríguez Ó., Napolitano N. R., Tortora C., 2019, MNRAS, 483, 3888
Suyu S. H. et al., 2013, ApJ, 766, 70
The Dark Energy Survey Collaboration, 2005, preprint (arXiv:astro-ph/0510346)
Treu T., Marshall P. J., 2016, A&AR, 24, 11
Treu T. et al., 2018, MNRAS, 481, 1041
Walsh D., Carswell R. F., Weymann R. J., 1979, Nature, 279, 381
Warren S. J. et al., 2007, preprint (arXiv:astro-ph/0703037)
Williams P., Agnello A., Treu T., 2017, MNRAS, 466, 3088
Wisotzki L., Koehler T., Groote D., Reimers D., 1996, A&AS, 115, 227
Wisotzki L., Christlieb N., Liu M. C., Maza J., Morgan N. D., Schechter P. L., 1999, A&A, 348, L41
Witt H. J., Mao S., Keeton C. R., 2000, ApJ, 544, 98
Wright E. L. et al., 2010, AJ, 140, 1868
Wynne R. A., Schechter P. L., 2018, preprint (arXiv:1808.06151)
York D. G. et al., 2000, AJ, 120, 1579

APPENDIX: LIST OF HIGH-GRADED CANDIDATES

In Tables A1 and A2, we provide a list of high-graded lensed quasars candidates found with these searches over DES-DR1, divided by search method. The magnitudes are from *WISE* and *Gaia*-DR1 and given in the Vega system.

[13]See https://des.ncsa.illinois.edu/thanks for full list of Collaborating Institutions.

Table A1. List of candidates recovered by the methods based on optical colours and spectra described in Section 2.

Object name	W1	W2	W3	G	Methods	Other
J000128.98−554959.1	14.93 ± 0.03	14.17 ± 0.04	11.85 ± 0.23	19.39	W2MG1mult	
J005301.98+002043.2	15.13 ± 0.04	14.02 ± 0.05	11.75 ± 0.34	17.65	W2MG1sing	PanSTARRS
J011455.07−054753.7	14.92 ± 0.04	14.59 ± 0.06	10.73 ± 0.10	19.91	W2MG1mult	PanSTARRS
J011509.25−231453.5	14.41 ± 0.03	14.06 ± 0.04	11.51 ± 0.18	19.14	W2MG1sing	PanSTARRS
J020157.21−051000.9	14.79 ± 0.03	14.35 ± 0.04	11.47 ± 0.15	19.92	W2MG1sing	PanSTARRS
J021524.18−472845.0	14.41 ± 0.03	13.33 ± 0.03	10.04 ± 0.05	18.60	W2MG1sing	
J023207.66−325458.1	14.95 ± 0.03	14.59 ± 0.05	11.76 ± 0.18	19.13	W2MG1mult	KiDS
J023639.92−475231.6	14.06 ± 0.03	13.31 ± 0.03	9.95 ± 0.05	20.13	W2MG1sing	
J030606.05−611130.0	15.22 ± 0.03	14.78 ± 0.04	10.61 ± 0.07	20.31	W2MG1sing	
J033908.87−612144.7	14.61 ± 0.03	13.44 ± 0.03	10.26 ± 0.05	18.45	W2MG1mult	
J035542.64−533440.3	14.31 ± 0.03	13.56 ± 0.03	9.92 ± 0.03	20.23	W2MG1sing	
J040148.10−251438.0	14.17 ± 0.03	13.12 ± 0.03	10.20 ± 0.06	18.79	W2MG1sing	PanSTARRS
J041848.07−275410.1	14.34 ± 0.03	13.88 ± 0.03	10.21 ± 0.05	19.85	W2MG1mult	PanSTARRS
J045453.01−302636.0	14.85 ± 0.03	14.48 ± 0.04	11.33 ± 0.13	18.79	W2MG1sing	PanSTARRS
J050120.31−633247.8	13.47 ± 0.02	12.54 ± 0.02	9.75 ± 0.03	20.58	W2MG1sing	
J215713.63−420149.5	12.40 ± 0.02	11.16 ± 0.02	8.65 ± 0.02	17.84	W2MG1sing	
J003247.75−243429.0	16.39 ± 0.06	15.99 ± 0.15	11.98	19.89	*Gaia*DR2mult	
J004254.16+045254.2	14.06 ± 0.03	13.81 ± 0.05	11.49	18.27	*Gaia*DR2mult	PanSTARRS
J005813.40−394724.6	14.77 ± 0.03	14.05 ± 0.04	11.23 ± 0.12	19.42	GaiaDR2mult	PanSTARRS
J012325.25−204852.9	14.68 ± 0.03	14.37 ± 0.05	11.94	18.78	*Gaia*DR2mult	PanSTARRS
J015033.23−030746.5	15.97 ± 0.05	14.83 ± 0.07	11.53 ± 0.20	20.07	*Gaia*DR2mult	PanSTARRS
J024754.77−634923.2	15.10 ± 0.03	14.36 ± 0.04	11.44 ± 0.11	19.68	GaiaDR2mult	
J041137.60−483935.8	14.71 ± 0.03	14.42 ± 0.03	11.83 ± 0.13	18.98	*Gaia*DR2mult	
J052611.27−393346.6	15.47 ± 0.04	14.74 ± 0.05	11.65 ± 0.16	19.98	GaiaDR2mult	
J060832.98−351309.7	15.47 ± 0.04	14.39 ± 0.04	11.34 ± 0.12	20.05	GaiaDR2mult	
J212034.78−423904.7	14.82 ± 0.03	13.71 ± 0.04	10.83 ± 0.11	19.37	*Gaia*DR2mult	
J201425.41−595746.6	14.81 ± 0.03	13.91 ± 0.04	11.17 ± 0.13	17.56	GaiaDR2mult	
J202649.74−422818.6	14.83 ± 0.04	13.99 ± 0.05	11.24 ± 0.16	19.70	GaiaDR2mult	
J203348.67−593640.1	13.28 ± 0.02	12.55 ± 0.02	10.04 ± 0.05	19.99	*Gaia*DR2mult	
J210014.9−445206.4	14.14 ± 0.03	13.42 ± 0.03	10.74 ± 0.10	18.79	*Gaia*DR2mult	
J211242.15−595924.2	14.98 ± 0.03	14.44 ± 0.05	10.70 ± 0.10	17.76	GaiaDR2mult	
J212354.86+004416.2	16.04 ± 0.06	15.66 ± 0.14	11.87	–	*Gaia*DR2mult	PanSTARRS
J215021.33−565008.5	16.14 ± 0.11	15.76 ± 0.18	11.57	20.30	GaiaDR2mult	
J215431.92−444302.0	14.63 ± 0.03	14.35 ± 0.05	11.68	19.18	*Gaia*DR2mult	
J215837.29−581203.9	14.70 ± 0.03	13.87 ± 0.03	11.52 ± 0.17	19.67	GaiaDR2mult	
J220819.74−631500.9	15.00 ± 0.03	14.70 ± 0.06	11.66	19.31	GaiaDR2mult	
J001947.71−293255.2	16.33 ± 0.07	16.47 ± 0.24	12.16	–	2QZ	KiDS/PanSTARRS
J003503.89−313203.2	17.73 ± 0.20	16.68	12.36	–	2QZ	KiDS
J023023.47−281003.3	16.54 ± 0.07	16.00 ± 0.14	12.60 ± 0.42	–	2QZ	KiDS/PanSTARRS
J023221.00−314913.1	–	–	–	–	2QZ	
J025001.69−373244.7	14.58 ± 0.03	13.74 ± 0.03	9.26 ± 0.03	–	6dFGS	
J030403.03−195524.4	15.86 ± 0.04	14.76 ± 0.05	10.28 ± 0.06	–	6dFGS	PanSTARRS
J053009.04−383734.9	15.18 ± 0.03	14.26 ± 0.04	9.97 ± 0.04	–	6dFGS	

Table A2. List of candidates recovered by the methods described in Section 2, based on X-ray and Radio data.

Object name	W1	W2	W3	G	Methods	Other
J002453.30−271644.0	15.53 ± 0.04	14.82 ± 0.07	11.96 ± 0.33	20.21	RASS	KiDS/PanSTARRS
J004123.99−252944.9	15.16 ± 0.04	14.76 ± 0.06	11.66 ± 0.20	–	RASS	PanSTARRS
J004659.57+042039.0	15.53 ± 0.05	15.23 ± 0.12	11.72 ± 0.42	–	RASS	PanSTARRS
J005044.12−524856.5	14.53 ± 0.03	13.78 ± 0.03	11.06 ± 0.13	20.75	RASS	
J005911.01−015544.5	15.41 ± 0.04	15.13 ± 0.10	11.60 ± 0.31	–	RASS	PanSTARRS
J010515.03−625238.5	15.64 ± 0.04	14.92 ± 0.05	12.46 ± 0.39	–	RASS	
J011226.92−252032.2	14.55 ± 0.03	13.86 ± 0.04	11.41 ± 0.15	–	RASS	PanSTARRS
J014802.99−210841.6	16.07 ± 0.06	15.80 ± 0.15	12.47	–	RASS	PanSTARRS
J020807.24−183910.9	14.42 ± 0.03	14.12 ± 0.04	12.08	–	RASS	PanSTARRS
J021039.97−341941.8	15.34 ± 0.04	15.03 ± 0.07	12.23	19.41	RASS	KiDS
J021307.50−364715.5	16.16 ± 0.05	15.95 ± 0.13	12.31	20.70	RASS	
J023208.04−640931.6	16.13 ± 0.05	15.92 ± 0.10	13.11		RASS	
J023225.72−295737.1	17.43 ± 0.15	16.03 ± 0.14	12.51	–	RASS	KiDS/PanSTARRS
J023919.80−470108.9	16.73 ± 0.07	15.98 ± 0.11	11.73 ± 0.17	–	RASS	

Table A2 – *continued*

Object name	W1	W2	W3	G	Methods	Other
J030034.07−494237.4	13.76 ± 0.02	12.73 ± 0.02	9.89 ± 0.05	18.09	RASS	
J032354.51−104649.3	17.75 ± 0.18	16.83	12.14	–	RASS	PanSTARRS
J033514.21−600808.5	14.02 ± 0.03	12.87 ± 0.02	10.03 ± 0.04	17.55	RASS	
J033656.27−154756.5	15.55 ± 0.04	15.16 ± 0.07	12.14	–	RASS	PanSTARRS
J034732.60−175324.0	15.03 ± 0.03	14.67 ± 0.05	11.52 ± 0.20	–	RASS	PanSTARRS
J035546.66−214818.5	15.56 ± 0.04	14.85 ± 0.06	11.08 ± 0.12	–	RASS	PanSTARRS
J043801.62−622942.9	15.85 ± 0.04	15.46 ± 0.07	12.58 –	–	RASS	
J044808.16−184642.3	15.36 ± 0.04	14.44 ± 0.05	10.58 ± 0.07	–	RASS	PanSTARRS
J045045.35−641642.8	16.74 ± 0.05	15.70 ± 0.07	13.24 ± 0.46	–	RASS	
J053248.87−391759.1	13.57 ± 0.02	12.62 ± 0.02	10.37 ± 0.06	19.92	RASS	
J215029.44−020016.9	15.18 ± 0.04	14.89 ± 0.08	11.05 ± 0.15	–	RASS	PanSTARRS
J225915.21−485056.2	15.50 ± 0.04	14.83 ± 0.06	10.81 ± 0.11	–	RASS	
J231409.88−421549.6	13.87 ± 0.03	12.71 ± 0.03	9.60 ± 0.04	–	RASS	
J235111.37−375323.5	14.79 ± 0.03	13.77 ± 0.04	11.57 ± 0.19	18.86	RASS	
J055640.64−611521.3	14.76 ± 0.03	13.82 ± 0.03	11.58 ± 0.10	19.50	XMMslew	
J000806.23−561551.9	16.26 ± 0.06	15.87 ± 0.13	11.50 ± 0.17	–	SUMSS	
J010844.90−315335.7	14.87 ± 0.03	14.59 ± 0.05	12.56	–	SUMSS	KiDS
J012043.82−631556.5	13.95 ± 0.03	12.69 ± 0.03	9.36 ± 0.03	–	SUMSS	
J013506.97−412612.0	11.91 ± 0.03	11.25 ± 0.02	6.04 ± 0.01	17.87	SUMSS	
J020722.82−533224.1	15.72 ± 0.04	15.21 ± 0.06	11.71 ± 0.17	–	SUMSS	
J022238.34−531958.2	16.07 ± 0.05	15.64 ± 0.09	12.23	–	SUMSS	
J025310.73−552823.2	16.13 ± 0.05	15.75 ± 0.09	12.07 ± 0.23	–	SUMSS	
J032028.96−530944.7	14.80 ± 0.03	14.50 ± 0.04	12.87	–	SUMSS	
J035425.21−642344.5	13.12 ± 0.02	11.95 ± 0.02	8.30 ± 0.02	–	SUMSS	
J042936.07−582237.5	16.05 ± 0.03	15.71 ± 0.05	12.24 ± 0.15	–	SUMSS	
J043228.41−545853.8	15.59 ± 0.03	14.82 ± 0.04	12.76 ± 0.24	–	SUMSS	
J044242.88−481249.5	16.12 ± 0.05	15.70 ± 0.09	12.75	–	SUMSS	
J045947.39−641538.9	15.39 ± 0.03	14.84 ± 0.04	12.84 ± 0.35	19.76	SUMSS	
J050309.96−311652.0	15.89 ± 0.04	15.62 ± 0.08	12.88	–	SUMSS	
J050709.35−465931.8	16.18 ± 0.05	15.77 ± 0.09	12.98	–	SUMSS	
J051052.38−520129.2	15.34 ± 0.03	14.98 ± 0.05	12.84	19.31	SUMSS	
J053128.21−383954.3	17.91 ± 0.18	17.50 ± 0.44	–	–	SUMSS	
J211006.51−484121.1	16.21 ± 0.06	15.77 ± 0.12	12.49 ± 0.45	–	SUMSS	
J215533.59−483645.2	16.74 ± 0.09	16.21 ± 0.19	12.06 ± 0.35	–	SUMSS	
J225710.84−535824.9	15.45 ± 0.04	15.13 ± 0.08	12.32 ± 0.42	19.59	SUMSS	
J222136.92−574847.6	15.10 ± 0.04	14.44 ± 0.04	12.20 ± 0.33	–	SUMSS	
J233432.25−585646.7	15.71 ± 0.04	15.41 ± 0.09	12.32 ± 0.42	–	SUMSS	
J234038.36−461254.8	16.27 ± 0.06	15.66 ± 0.11	12.17 ± 0.33	–	SUMSS	
J234721.48−561943.7	15.46 ± 0.04	15.17 ± 0.06	12.42	–	SUMSS	
J234839.67−520936.5	14.61 ± 0.03	14.10 ± 0.04	12.10 ± 0.34	–	SUMSS	
J235311.68−544823.3	16.80 ± 0.09	15.84 ± 0.13	11.96	–	SUMSS	

This paper has been typeset from a TEX/LATEX file prepared by the author.